Bioorganic Chemistry 86 (2019) 224–234

Contents lists available at ScienceDirect

Bioorganic Chemistry

journal homepage: www.elsevier.com/locate/bioorg

Discovery of potent PTP1B inhibitors via structure-based drug design, synthesis and *in vitro* bioassay of Norathyriol derivatives

Wenjie Xue[a], Jinlong Tian[a], Xiang Simon Wang[b], Jie Xia[a,*], Song Wu[a,*]

[a] State Key Laboratory of Bioactive Substance and Function of Natural Medicines, Department of New Drug Research and Development, Institute of Materia Medica, Chinese Academy of Medical Sciences and Peking Union Medical College, Beijing 100050, China
[b] Department of Pharmaceutical Sciences, College of Pharmacy, Howard University, Washington DC 20059, USA

ARTICLE INFO

Keywords:
PTP1B inhibitors
Structure-based drug design
Molecular docking
Norathyriol

ABSTRACT

Protein tyrosine phosphatase 1B (PTP1B) has recently been identified as a potential target of Norathyriol. Unfortunately, Norathyriol is not a potent PTP1B inhibitor, which somewhat hinders its further application. Based on the fact that no study on the relationship of chemical structure and PTP1B inhibitory activity of Norathyriol has been reported so far, we attempted to perform structural optimization so as to improve the potency for PTP1B. Via structure-based drug design (SBDD), a rational strategy based on the binding mode of Norathyriol to PTP1B, we designed 26 derivatives with substitutions at the four phenolic hydroxyl groups of Norathyriol. By chemical synthesis and *in vitro* bioassay, we identified seven PTP1B inhibitors that were more potent than Norathyriol, of which **XWJ24** showed the highest potency (IC_{50}: 0.6 μM). We also found out that **XWJ24** was a competitive inhibitor and showed the 4.5-fold selectivity over its close homolog, TC-PTP. Through molecular docking of **XWJ24** against PTP1B, we highlighted the essential role of its hydrogen bond with Asp181 for PTP1B inhibition and identified a potential halogen bond with Asp48 that was not observed for Norathyriol. The current data indicate that our SBDD strategy is effective to discover potent PTP1B-targeted Norathyriol derivatives, and **XWJ24** is a promising lead compound for further development.

1. Introduction

Protein tyrosine kinases (PTKs) and protein tyrosine phosphatases (PTPs) are two large families of enzymes that regulate tyrosine phosphorylation levels with opposite functions. PTKs function to catalyze tyrosine phosphorylation, while PTPs are responsible for de-phosphorylation of phosphorylated proteins on tyrosine [1,2]. Since tyrosine phosphorylation and de-phosphorylation play key roles in signal transduction pathways that are essential for cellular processes, the dysfunction of either PTKs or PTPs may result in the development of various human diseases, in particular diabetes and cancers [3]. Accordingly, both PTKs and PTPs have emerged as promising targets for drug discovery and development. Targeting PTKs has been proved successful as drugs targeting PTKs are in clinical use [4], while PTPs-targeted drug discovery still faces a great challenge [5].

In the family of PTPs, PTP1B is the first purified PTP [6] and the most studied. In terms of its classification, it belongs to class I cysteine-based family, precisely the intercellular, non-receptor subfamily [1]. PTP1B has long been an attractive therapeutic target in the treatment of type II diabetes and obesity [7], since the first discovery of its role in the negative regulation of insulin signal transduction through the de-phosphorylation of insulin receptor [8] and the demonstration of improved insulin sensitivity in PTP1B-knockout mouse model [9]. Due to its wide expression in tissues and involvement in almost all physiological responses, PTP1B is suggested as a promising target in various disorders [10] such as liver diseases [11], cardiovascular diseases [12], cancer (especially breast cancer) [13,14] and even in the X-linked neurological disorder Rett syndrome [15].

The role that PTP1B plays in the progression of diseases propels to the discovery of a great number of PTP1B inhibitors, including both

Abbreviations: PTKs, Protein tyrosine kinases; PTPs, protein tyrosine phosphatases; SBDD, structure-based drug design; PDB, Protein Data Bank; SAR, structure-activity relationship; TCPTP, T-cell PTP; SHP2, Src homology region 2-containing PTP 2; PTP-LAR, leukocyte antigen-related PTP; m.p., melting points; HRMS, high resolution electrospray ionization mass spectra; TLC, thin layer chromatography; DTT, dithiothreitol; DiFMUP, 6,8-Difluoro-4-Methylumbelliferyl Phosphate; FI, fluorescence intensity

* Corresponding authors at: Department of New Drug Research and Development, Institute of Materia Medica, Chinese Academy of Medical Sciences, No. 2 Nanwei Rd, Beijing 100050, China.
E-mail addresses: jie.william.xia@hotmail.com (J. Xia), ws@imm.ac.cn (S. Wu).

https://doi.org/10.1016/j.bioorg.2019.01.059
Received 24 September 2018; Received in revised form 11 January 2019; Accepted 27 January 2019
Available online 28 January 2019

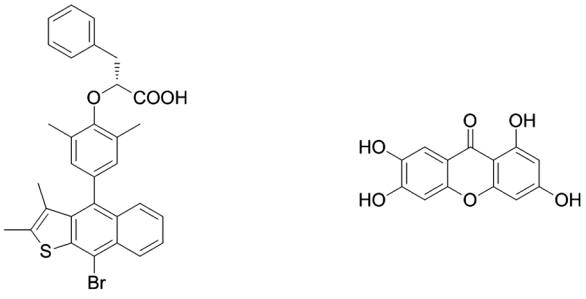

Ertiprotafib

lauched Phase I clinical trial in 2000
discontinued in Phase II clinical trial in 2002

Norathyriol

Fig. 1. The chemical structures of Ertiprotafib, the first PTP1B inhibitor that enters a clinical trial, and Norathyriol, a PTP1B-targeted natural product.

synthetic molecules and natural products [16–18]. Among them, Ertiprotafib is the first to enter a clinical trial for the treatment of diabetes, but it fails in the following Phase II clinical trial in 2002 due to its insufficient efficacy and undesirable side effects [7]. Until now, there is still no PTP1B inhibitor on the drug market. Therefore, novel PTP1B inhibitors remain to be much-needed as they may show advantages over Ertiprotafib.

Norathyriol is a natural product isolated from plants such as mango, Hypericum elegans, and Tripterospermum lanceolatum (cf. Fig. 1). Due to its wide range of biological activities (e.g. antioxidant, anti-inflammatory, antitumor and anti-diabetes activities [19]), this compound attracts much interest which mainly focuses on its underlying mechanism regarding targets and biological pathways [19–24]. Recently, Ding, H. et al. demonstrated for the first time that Norathyriol reverses obesity- and high-fat-diet-induced insulin resistance in mice through the PTP1B inhibition in a competitive way [22]. Their report indicates Norathyriol is a PTP1B inhibitor that binds to the catalytic site. Though Norathyriol is not potent *in vitro* (IC_{50} value: 9.59 μM), it possesses good cell permeability and oral availability.

Up to now, no effort on structural optimization of Norathyriol to improve PTP1B inhibition has been undertaken. In this study, we aim to improve its *in vitro* potency by applying structure-based drug design (SBDD) strategy, because crystal structures of PTP1B in complex with its inhibitors are available to use. Firstly, Norathyriol was docked against the catalytic site of PTP1B (Protein Data Bank (PDB) Entry: 1Q1M). Based on a plausible binding mode, we designed and synthesized a series of derivatives with substitutions of four phenolic hydroxyl groups at the 1-, 3-, 6- and 7-positions of Norathyriol. Then, we tested the Norathyriol derivatives for their inhibitory activity on PTP1B and studied the type of enzymatic inhibition and selectivity profile of the most potent derivative, i.e. **XWJ24**. Lastly, we proposed a plausible binding mode of **XWJ24** to PTP1B according to the predictions from molecular docking and the structure-activity relationship, which will guide further optimization.

2. Results and discussions

2.1. SBDD based on the binding mode of Norathyriol

The work was aimed to discover PTP1B inhibitors that are more potent than Norathyriol. With the high-resolution crystal structures of PTP1B available in PDB, we applied the structure-based drug design strategy to the structural optimization of Norathyriol. The molecular docking against PTP1B indicates that Norathyriol fits into the catalytic site well while its hydroxyl group at the 3-position stretched towards site 2, which were mostly hydrophobic (cf. Fig. 2A). The binding mode of Norathyriol includes four plausible interactions: (1) hydrogen bond between the hydroxyl groups at the 6- and the 7- positions and Asp181; (2) π-π stacking interactions between the aromatic rings and Phe182 as well as between the aromatic rings and Tyr46; (3) σ-π interaction between the aromatic ring and Val49 as well as Ala217; (4) hydrogen bond between the hydroxyl group at the 3-position and Asp48. Accordingly, we decided to synthesize Norathyriol derivatives by modifying four hydroxyl groups at the 1-, 3-, 6- and 7-positions as they were easy to prepare. According to the binding mode, we hypothesized that the introduction of certain lipophilic groups to the phenolic hydroxyl group at the 3-position may improve potency, thus we designed **XWJ6**-**XWJ10** with substituted carbamoyl groups and **XWJ15**-**XWJ24** with substituted benzyl groups. Also, it seemed that the modification at other hydroxyl groups may lower down the potency, thus we designed **XWJ1**-**XWJ5** with substituted carbamoyl groups at the 1-position, **XWJ11**-**XWJ14** with substituted carbamoyl groups at the 1- and the 3-positions and **XWJ25**-**XWJ26** with benzyl groups at 3-, 6- and 7-positions so as to probe the interactions between Norathyriol and PTP1B.

2.2. Chemistry

A total of 26 Norathyriol derivatives (cf. Table 1) were synthesized and their chemical structures were validated by melting points, HR MS, ^{1}H NMR and ^{13}C NMR. All compounds described herein were prepared as outlined in Schemes 1-4. The compounds named **XWJ1**-**XWJ5** bearing substituted carbamate at the 1-position were prepared as outlined in Scheme 1, which consists of the protection of the hydroxyl groups at the 3-, 6- and 7-positions with chloromethyl methyl ether, the carbamatation at the 1-position and the deprotection. All the 3-substituted carbamoyl Norathyriol derivatives (i.e. **XWJ6**-**XWJ10**) were prepared according to Scheme 2. In this scheme, the Norathyriol firstly reacts with dichlorodiphenyl methane in high-boiling diphenyl ether to afford a high yield of protected intermediate. Then the intermediate is carbamylated in acetone and deprotected via palladium-carbon catalytic hydrogenation, which renders the final products. The compounds **XWJ11**-**XWJ14** were prepared as outlined in Scheme 3, which starts from the reaction between the dichlorodiphenylmethylene-protecting Norathyriol and an excessive amount of substituted carbamyl chloride and ends with the deprotection. The general procedure to prepare the compounds **XWJ15**-**XWJ24** is described in Scheme 4, where Norathyriol reacts with a certain amount of substituted benzyl bromide in a manner of one-pot method. The synthesis of **XWJ25**-**XWJ26** was based on the same procedure as that of **XWJ15**-**XWJ24** except for the use of an excessive amount of substituted benzyl bromide.

2.3. Biology

2.3.1. PTP1B inhibition and Structure-activity relationship (SAR)

All the synthesized Norathyriol derivatives were tested for their *in vitro* PTP1B inhibitory activity, with Na_3VO_4 as the positive drug and Norathyriol as a reference. Their corresponding inhibition rates and/or IC_{50} values are shown in Table 1. Seven Norathyriol derivatives, i.e. **XWJ8**, **XWJ9**, **XWJ10**, **XWJ12**, **XWJ14**, **XWJ15** and **XWJ24** showed inhibition rates greater than 50% on PTP1B at the concentration of 10 μM. Among them, the most potent derivative was **XWJ24** (IC_{50}: 0.6 μM) while the weakest was **XWJ8** (IC_{50}: 16.5 μM). The discovery of these derivatives that showed better activity than Norathyriol (IC_{50}: 25.9 μM) indicates that our SBDD strategy was effective in the optimization of Norathyriol.

The compounds named **XWJ1**-**XWJ5** are the Norathyriol derivatives with different carbamoyl groups at the 1-position. As shown in Table 1, the rank order of these compounds by inhibition rates is as follows: **XWJ1** (41%) > **XWJ3** (37%) > Norathyriol (29%) > **XWJ4** (26%) > **XWJ2** (19%) > **XWJ5** (14%). According to the structure and the activity, it can be concluded that: (1) the substitution with bulky hydrophobic groups seemed not favorable for PTP1B inhibition (e.g. **XWJ4** and **XWJ5**), while the introduction of small substituent groups may slightly improve potency (e.g. **XWJ1** and **XWJ3**); (2) the

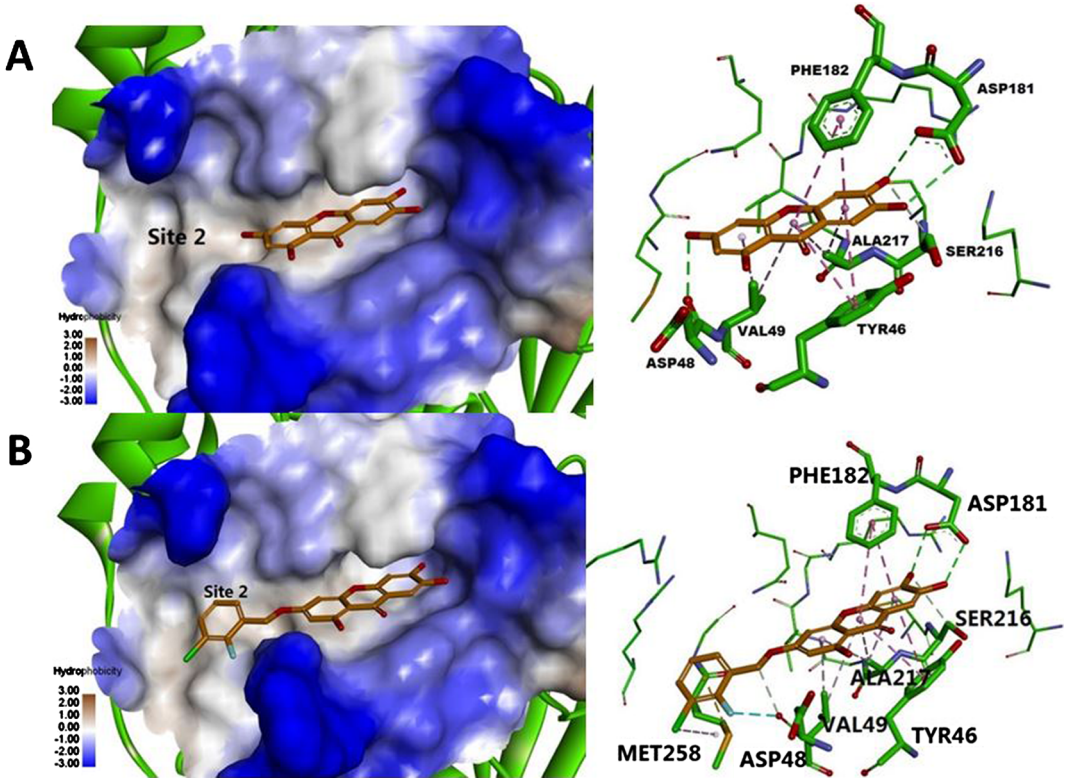

Fig. 2. Binding modes of Norathyriol (A) and **XWJ24** (B) to PTP1B. Color codes and representations: green and bold stick, the amino acid residues that interact with Norathyriol; orange stick, Norathyriol or **XWJ24**; blue surface, the most hydrophilic; brown surface, the most hydrophobic.

substitution at the 1-position may not represent an optimal strategy to improve potency, as the inhibition rates of all the compounds in this series are less than 50%.

When the same substituents were respectively introduced to the phenolic hydroxyl group at the 3-position, all the five derivatives were more potent than Norathyriol. To be noted, three of them showed potent inhibition on PTP1B with the inhibition rates over 50%. The most potent one was **XWJ10**, with an IC_{50} value of 4.3 μM. Unlike the SAR of the derivatives with substituents at the 1-position, the potency went up with the increase in the size of the hydrophobic substituents at the 3-position. For instance, compared to **XWJ6** (dimethylcarbamate) and **XWJ7** (ethyl(methyl)carbamate), **XWJ8** (diethylcarbamate), **XWJ9** (morpholine-4-carboxylate) and **XWJ10** (diphenylcarbamate) showed stronger PTP1B inhibition. It indicates the introduction of bulky hydrophobic carbamoyl groups at the 3-position may enhance potency. According to the SAR here and the binding mode of Norathyriol (cf. Fig. 2), it can be inferred that that hydrogen bond between Norathyriol and Asp48 may not be essential for PTP1B inhibition.

Based on the above SAR, we hypothesized that further introduction of the same substituents to the 1-position of the 3-monosubstituted Norathyriol derivatives (**XWJ7**-**XWJ10**) may have a similar effect to that on Norathyriol. To test our hypothesis, we synthesized four representative compounds (i.e. **XWJ11**-**XWJ14**) and tested their PTP1B inhibitory activity (cf. Table 1). Generally, the further substitution at the 1-position with small-size hydrophobic groups slightly improved PTP1B inhibition. For instance, the IC_{50} values were 8.3 μM for **XWJ12** and 16.5 μM for **XWJ7**. By contrast, the substitution with bulky hydrophobic groups at the corresponding position reduced its inhibition on PTP1B. To be specific, the bis(morpholine-4-carboxylate) was not active (**XWJ13** with an inhibition rate of 25%) while the morpholine-4-carboxylate was a potent PTP1B inhibitor (**XWJ9** with an IC_{50} value of 10.8 μM). The potency of bisdiphenylcarbamate (**XWJ14**: 9.9 μM) was half that of diphenylcarbamate (**XWJ10**: 4.3 μM). These data validate the effect of the substitutions at the 1-position.

As **XWJ10** was the most potent PTP1B inhibitor in the carbamates, it seemed the 3-position mono-substitutions with aromatic hydrophobic groups were more effective in improving potency than the 1-position mono-substitutions and 1,3-positions disubstitutions, thus we introduced various substituted benzyl groups to the 3-hydroxyl group of Norathyriol. In this series, only the introduction of the p-methyl (**XWJ15**) and 2-fluoro-3-chloro benzyl groups (**XWJ24**) brought about improved potency, compared with Norathyriol. To be specific, **XWJ24** exhibited sub-micromolar potency (IC_{50} = 0.6 μM), which was over 40 times that of Norathyriol. **XWJ15** also showed great PTP1B inhibition, which an IC_{50} value of 1.2 μM.

In order to explore the importance of 6,7-bishydroxyl group of Norathyriol to PTP1B activity, we selected two derivatives with benzyl groups, i.e. **XWJ15** and **XWJ18** as representative molecules. The former was a potent PTP1B inhibitor, while the latter was quite weak (with an inhibition rate of 21%). The further introduction of *p*-methyl or *p*-chloro benzyl group to the 6- and 7- positions resulted in the complete loss of potency, suggesting the essential role of the two hydroxyl groups of Norathyriol in maintaining PTP1B inhibitory activity. The explanation for that could be the loss of the hydrogen bond between Norathyriol and Asp181 (cf. Fig. 2A).

2.3.2. The type of PTP1B inhibition

In order to uncover how Norathyriol derivatives bound to PTP1B, we performed PTP1B kinetics bioassay and used Lineweaver-Burk plot to determine the type of PTP1B inhibition. As shown in Fig. 3, four lines representing the effects of the compound from low to high concentration show the changes of slopes and x-intercepts in the same trend but unchanged y-intercept. It indicates Vmax (i.e. maximum reaction velocity) was not affected by the compound concentration, while the Km increased with the compound concentration. Based on these features, **XWJ24** was confirmed as a competitive inhibitor. Thus, **XWJ24** was supposed to bind to PTP1B at the catalytic site, the same as Norathyriol does [22].

Table 1
The chemical structures and PTP1B inhibitory activities of 26 Norathyriol derivatives.

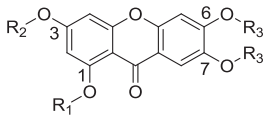

Cmpd. ID.	R_1	R_2	R_3	Inhibition rate (%) at 10 μM	IC_{50} (μM, mean ± SD[a])
XWJ1		H	H	41	n.d.[b]
XWJ2		H	H	19	n.d.
XWJ3		H	H	37	n.d.
XWJ4		H	H	26	n.d.
XWJ5		H	H	14	n.d.
XWJ6	H		H	38	n.d.
XWJ7	H		H	44	n.d.
XWJ8	H		H	54	16.5 ± 1.1
XWJ9	H		H	59	10.8 ± 0.8
XWJ10	H	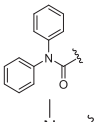	H	53	4.3 ± 0.3
XWJ11	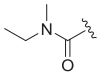	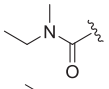	H	36	n.d.
XWJ12	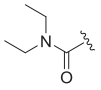	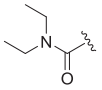	H	56	8.3 ± 0.8
XWJ13	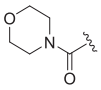	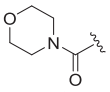	H	25	n.d.
XWJ14	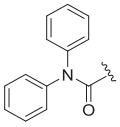	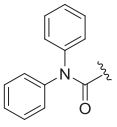	H	55	9.9 ± 0.4
XWJ15	H	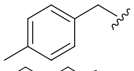	H	85	1.2 ± 0.1
XWJ16	H	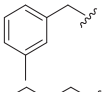	H	27	n.d.
XWJ17	H	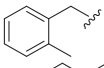	H	33	n.d.
XWJ18	H	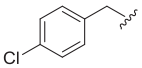	H	21	n.d.
XWJ19	H	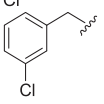	H	23	n.d.

(*continued on next page*)

Table 1 (*continued*)

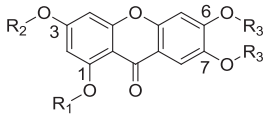

Cmpd. ID.	R_1	R_2	R_3	Inhibition rate (%) at 10 μM	IC_{50} (μM, mean ± SD[a])
XWJ20	H	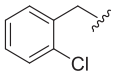	H	20	n.d.
XWJ21	H	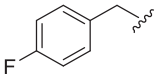	H	26	n.d.
XWJ22	H	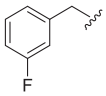	H	20	n.d.
XWJ23	H	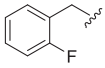	H	9	n.d.
XWJ24	H	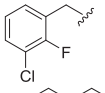	H	96	0.6 ± 0.1
XWJ25	H	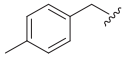	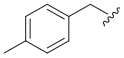	4	n.d.
XWJ26	H	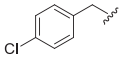	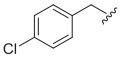	2	n.d.
Norathyriol	H	H	H	29	25.9 ± 2.3[c]
Na_3VO_4	–	–	–	–	2.4 ± 0.2

[a] mean, the average of duplicate; SD, standard deviation.
[b] n.d., not determined. IC_{50} values were not determined for the compounds whose PTP1B inhibition rates were less than 50%.
[c] IC_{50} value reported by Ding, H. et al.: 9.59 μM.

2.3.3. Binding mode of ***XWJ24*** to PTP1B

In order to understand SAR in depth, we further performed molecular docking of the most potent inhibitor, i.e. **XWJ24** against PTP1B using the same parameters as that for Norathyriol. As shown in Fig. 2B, **XWJ24** bound to the catalytic site of PTP1B mostly in the same mode as Norathyriol. For instance, the hydrogen bond with Asp181, the π-π stacking with Phe182 as well as Tyr46 and σ-π interaction with Val49 as well as Ala217 still existed. The difference was that the nonessential hydrogen bond with Asp48 was replaced by a halogen bond between o-fluorine atom and Asp48. In addition, it seemed a plausible π-sulfur interaction between the phenyl group and Met258 and an alkyl-type hydrophobic interaction between the *m*-chloro atom and Met258 facilitated the binding of the benzyl group.

2.3.4. Inhibition of other PTPs activities by ***XWJ24***

We also tested the inhibitory activities of **XWJ24** against a panel of other PTPs, i.e. T-cell PTP (TC-PTP), Src homology region 2-containing PTP 2 (SHP2) and leukocyte antigen-related PTP (PTP-LAR), and compared its selectivity profile with that of Norathyriol. Norathyriol is somewhat selective to PTP1B over the other three PTPs, though it is very weak for those targets. In particular, no inhibition was observed for both TC-PTP and SHP2 (IC_{50} > 100 μM). After structural optimization, **XWJ24** potently inhibited PTP1B, SHP2 and PTP-LAR (IC_{50} value: 0.6 μM, 0.93 μM and 0.69 μM) and moderately inhibited TC-PTP (IC_{50} value: 2.7 μM). Though it was not selective to PTP1B over SHP2 or PTP-LAR, it showed 4.5-fold selectivity over the highly homologous TC-PTP. The comparison between the profiles of Norathyriol and **XWJ24** indicates that our SBDD strategy was feasible to improve potency while maintaining selectivity.

3. Conclusion

PTP1B has been recognized as a potential target in the treatment of various human diseases for a long time. Though a lot of efforts on drug discovery and development targeting PTP1B have been taken, no PTP1B inhibitor is marketed as a drug. Therefore, new chemical types

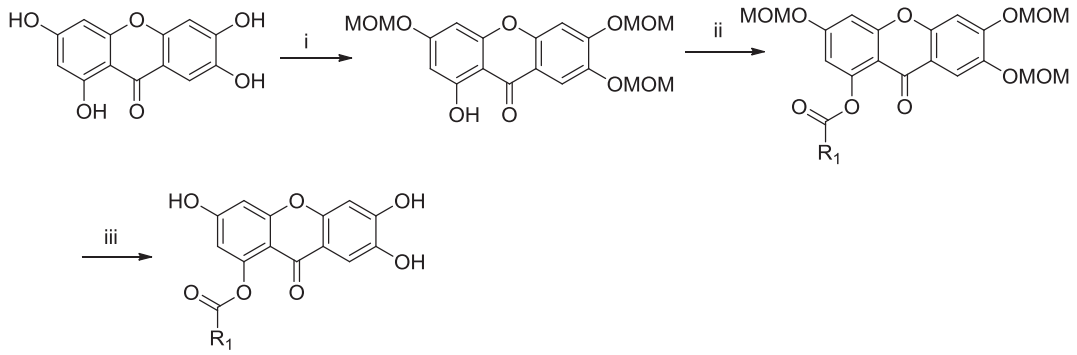

Scheme 1. Synthesis of **XWJ1**-**XWJ5**. Reagents and conditions: (i) $ClCH_2OCH_3$, DIEPA, CH_2Cl_2, 0 °C; (ii) CH_3COCH_3, Cs_2CO_3, R_1COCl, reflux; (iii) $CH_3CH_2OH{\cdot}HCl$, r.t.

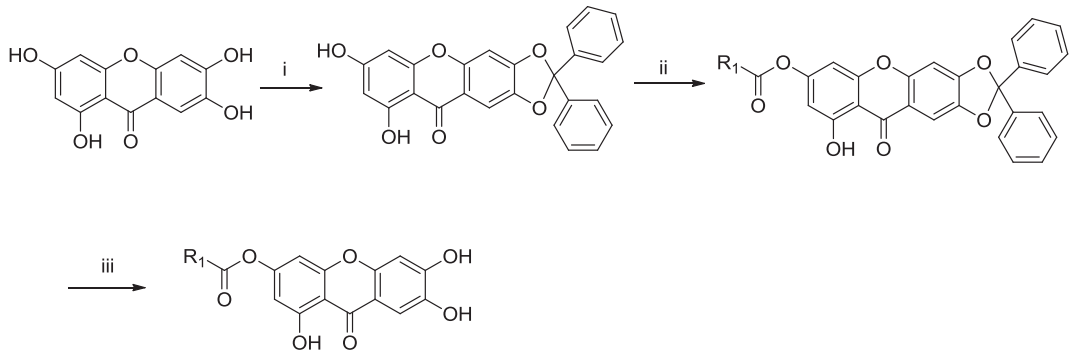

Scheme 2. Synthesis of **XWJ6**-**XWJ10**. Reagents and conditions: (i) dichlorodiphenyl methane, diphenyl ether, 175 °C; (ii) CH_3COCH_3, K_2CO_3, R_1COCl, reflux; (iii) THF/CH_3OH, H_2, Pd/C, 50 °C.

are still needed, as they may circumvent the weaknesses of currently available PTP1B inhibitors. Norathyriol, a natural product that can protect mice from diet-induced obesity and insulin resistance via oral administration [22], seems to represent such a new class of PTP1B inhibitors. Though it shows efficacy *in vivo*, PTP1B bioassay *in vitro* by Ding, H. et al. [22] and our group indicated that it is not a potent inhibitor. Based on the assumption that the improvement of inhibitory potency may lead to better *in vivo* outcome, we started this study to design, synthesize and test PTP1B-targeted Norathyriol derivatives.

Since SBDD, i.e. rational drug design based on 3D structures of a specific target has speeded up the discovery of many clinical drugs, it is widely acknowledged as a very powerful technique in early-stage drug discovery [25,26]. To apply it to PTP1B inhibitors design, we first used the available crystal structure of PTP1B (PDB ID: 1Q1M) for molecular docking and obtained plausible interactions between Norathyriol and PTP1B (cf. Fig. 1A). The binding mode implied that the potency may be improved by the modification at the phenolic hydroxyl group at the 3-position, thus we synthesized a series of derivatives and tested them by the *in vitro* PTP1B bioassay (cf. Table 1). The discovery of **XWJ24** as a much more potent PTP1B inhibitor than Norathyriol indicates the effectiveness of our SBDD strategy. Further kinetics assay confirmed that **XWJ24** is a competitive PTP1B inhibitor (cf. Fig. 3), and selectivity profiling demonstrated it is 4.5-fold selective to TC-PTP (cf. Table 2). Based on the SAR of Norathyriol derivatives and molecular docking, we reported a plausible binding mode of **XWJ24** to PTP1B, in which a halogen bond is involved in the interaction between **XWJ24** and Asp48 (cf. Fig. 2B). This halogen bonding can explain well the potency improvement from Norathyriol to **XWJ24**.

In summary, the present study describes the application of SBDD to the structural optimization of Norathyriol, which led to the discovery of a potent PTP1B inhibitor, i.e. **XWJ24**. It is worthwhile to further develop **XWJ24** into a series of highly potent and selective PTP1B inhibitors.

4. Materials and methods

4.1. Chemistry

4.1.1. General methods

All the materials were purchased from commercial suppliers and used without drying or purification, unless when necessary. Melting points (m.p.) were determined by a Melting Point YRT-3 apparatus (Tianjin University precision apparatus factory, China). The ^{1}H NMR (400 MHz or 500 MHz) and ^{13}C NMR spectra (100 MHz) were recorded by Bruker spectrometers (Varian Mercury, USA), with tetramethylsilane (TMS) as an internal standard. High resolution electrospray ionization mass spectra (HRMS) were recorded by Thermo Scientific™ Exactive™ Plus mass spectrometry (Thermo, USA). Reactions were monitored by thin layer chromatography (TLC) on silica gel sheets GF254 (Yantai Chemical Industry Research Institute, China). Spots were detected under ultraviolet light of 254 nm. The products were purified by column chromatography on silica gel (200–3000 mm; Qingdao Haiyang Chemical Co., Ltd, China).

4.1.2. General procedure A for the synthesis of 3,6,7-trihydroxy-9-oxo-9H-xanthen-1-yl carbamate (*XWJ1*-*XWJ5*)

N,N-Diisopropylethylamine (0.54 mL, 3.15 mmol) was added to a solution of Norathyriol (260.0 mg, 1.0 mmol) in dichloromethane. The mixture was stirred for 15 mins. Then, the chloromethyl methyl ether (0.24 mL, 3.15 mmol) was added under 0 °C. The resulting mixture was stirred at room temperature for 10 h. After that, the mixture was concentrated and purified using silica gel column chromatography, via which 1-hydroxy-3,6,7-tris(methoxymethoxy)-9*H*-xanthen-9-one was obtained as a light yellow solid in 81.6% yield. m.p.: 134.2–134.9 °C. ESI-MS (*m/z*): 393.24 $[M+H]^+$. ^{1}H NMR (400 MHz, DMSO -d_6) δ: 12.90 (s, 1H), 7.72 (s, 1H), 7.29 (s, 1H), 6.66 (d, J = 4 Hz, 1H), 6.46 (d, J = 4 Hz, 1H), 5.44 (s, 2H), 5.34 (s, 2H), 5.31 (s,2H), 3.45 (m, 6H), 3.42 (s, 3H). ^{13}C NMR (100 MHz, DMSO-d_6) δ: 179.99, 163.70, 163.22, 157.66, 153.83, 152.76, 144.35, 114.54, 110.88, 104.13, 103.58, 98.84, 95.78, 95.21, 94.37, 94.25, 56.69, 56.49.

An acetone (10 mL) solution of the intermediate from the last step (392.0 mg, 1.0 mmol), Cesium carbonate (1.0 g, 3.0 mmol) and Potassium iodide (166.0 mg, 1.0 mmol) was stirred at 50 °C for 1 h. Then the carbamyl chloride was slowly added and stirred for 8 h. The solvent was evaporated under reduced pressure, and the residual was partitioned between EtOAc and the saturated $NaHCO_3$ solution. The organic layer was washed with water, dried with anhydrous $MgSO_4$, filtered and concentrated under reduced pressure to afford crude oil. This product was dissolved in methanol (3 mL), followed by the addition of HCl/EtOH (5 mL, 2 M). The mixture was stirred at room temperature for 30 min, then concentrated and purified by silica gel chromatography (hexanes and EtOAc) to afford **XWJ1**-**XWJ5**.

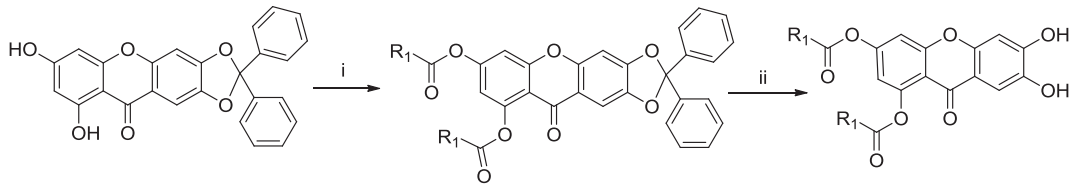

Scheme 3. Synthesis of **XWJ11**-**XWJ14**. Reagents and conditions: (i) CH_3COCH_3, Cs_2CO_3, R_1COCl, reflux; (ii) THF/CH_3OH, H_2, Pd/C, 50 °C.

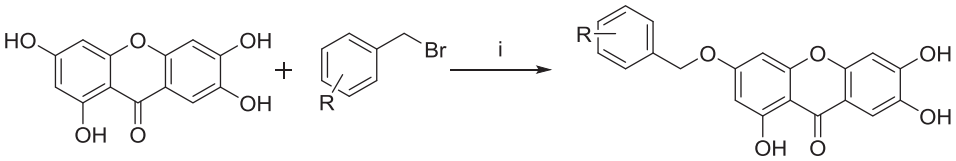

Scheme 4. Synthesis of **XWJ15**-**XWJ24**. Reagents and conditions: (i) $NaHCO_3$, DMF.

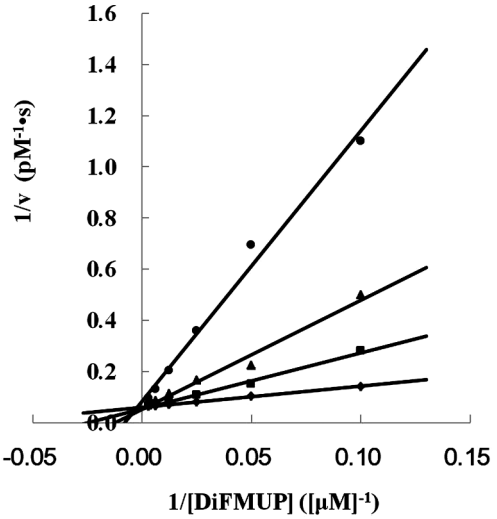

Fig. 3. The Lineweaver-Burk plot to determine the type of PTP1B inhibition. In the presence of **XWJ24** at the concentration of 0 μM (1% DMSO, rhombus), 0.2 μM (squares), 0.6 μM (triangles) or 1.8 μM (circles), the reciprocal of reaction velocity (1/v) was plotted against the reciprocal of DiFMUP concentration ((1/[DiFMUP]). The values are expressed as the average of duplicates.

Table 2
IC_{50} values of **XWJ24** and Norathyriol against a panel of protein tyrosine phosphatases (PTPs).

Cmpd. ID	IC_{50} (μM, mean ± SD[a])			
	PTP1B	TC-PTP	SHP2	PTP-LAR
XWJ24	0.6 ± 0.1	2.7 ± 0.2	0.93 ± 0.10	0.69 ± 0.04
Norathyriol	25.9 ± 2.3	> 100	> 100	79 ± 2
Na_3VO_4	2.4 ± 0.2	0.16 ± 0.05	0.71 ± 0.06	0.34 ± 0.03

[a] mean: the average of duplicate; SD, standard deviation.

*4.1.2.1. 3,6,7-trihydroxy-9-oxo-9H-xanthen-1-yl dimethylcarbamate (**XWJ1**).* Treatment of dimethylcarbamic chloride as outlined in general procedure A provided **XWJ1** as light yellow solids in 45.3% yield. ESI-MS (*m/z*): 332.01 $[M+H]^+$. ^1H NMR (400 MHz, DMSO-d_6) δ:7.31(s,1H), 6.82 (s,1H), 6.70 (d, J = 4 Hz, 1H), 6.47 (d, J = 4 Hz, 1H), 3.11 (s,3H), 2.92 (s,3H). ^{13}C NMR (100 MHz, DMSO-d_6) δ: 173.33, 162.45, 158.47, 154.42, 153.32, 152.53, 150.21, 143.87, 114.43, 109.37, 108.43, 108.33, 102.75, 100.32, 36.70. HRMS calcd for $C_{16}H_{14}NO_7$ $[M+H]^+$, 332.0765; found, 332.0765.

*4.1.2.2. 3,6,7-trihydroxy-9-oxo-9H-xanthen-1-yl ethyl(methyl)carbamate (**XWJ2**).* Treatment of ethyl(methyl)carbamic chloride as outlined in general procedure A provided **XWJ2** as light yellow solids in 28.5% yield. m.p.: 248.0–248.7 °C. ESI-MS (*m/z*): 345.92 $[M+H]^+$. ^1H NMR (400 MHz, DMSO-d_6) δ: 10.89(brs, 1H), 10.45(brs, 1H), 9.46(brs, 1H), 7.32(s, 1H), 6.82(s, 1H), 6.70(d, J = 4 Hz, 1H), 6.46(d, J = 4 Hz, 1H), 3.53–3.32(2 × q, J = 8 Hz, 2H), 3.08–2.90(2 × s, 3H), 1.29–1.12(2 × t, J = 8 Hz, 3H). ^{13}C NMR(100 MHz, DMSO-d_6) δ:173.27, 162.45, 158.47, 153.92, 153.25, 152.51, 150.19, 143.89, 114.45, 109.37, 108.60, 108.32, 102.77, 100.30, 43.99, 34.38, 12.82. HRMS calcd for $C_{17}H_{16}NO_7$ $[M+H]^+$, 346.0915; found, 346.0921.

*4.1.2.3. 3,6,7-trihydroxy-9-oxo-9H-xanthen-1-yl diethylcarbamate (**XWJ3**).* Treatment of diethylcarbamic chloride as outlined in general procedure A provided **XWJ3** as light yellow solids in 37.8% yield. m.p.: 223.7–224.5 °C. ESI-MS (*m/z*): 360.27 $[M+H]^+$. ^1H NMR (400 MHz, DMSO-d_6) δ: 10.86 (brs, 1H),10.44 (brs, 1H), 9.66 (brs, 1H), 7.32 (s, 1H), 6.82 (s, 1H), 6.70 (d, J = 4 Hz, 1H), 6.46 (d, J = 4 Hz, 1H), 3.51–3.46 (q, J = 8 Hz , 2H), 3.30 (q, J = 8 Hz , 2H), 1.29–1.26 (t, J = 8 Hz 3H), 1.16–1.12 (t, J = 8 Hz 3H). ^{13}C NMR (100 MHz, DMSO-d_6) δ: 173.18, 162.38, 158.47, 153.53, 153.18, 152.46, 150.17, 143.84, 114.47, 109.36, 108.62, 108.33, 102.76, 100.31, 41.98, 14.35, 13.73. HRMS calcd for $C_{18}H_{18}NO_7$ $[M+H]^+$, 360.1071; found, 360.1078.

*4.1.2.4. 3,6,7-trihydroxy-9-oxo-9H-xanthen-1-yl morpholine-4-carboxylate (**XWJ4**).* Treatment of morpholine-4-carbonyl chloride as outlined in general procedure A provided **XWJ4** as light yellow solids in 40.2% yield. m.p.: > 250 °C. ESI-MS (*m/z*): 374.51 $[M+H]^+$. ^1H NMR (400 MHz, DMSO-d_6) δ: 10.98 (brs, 1H), 10.47 (brs, 1H), 9.61 (brs, 1H), 7.35 (s, 1H), 6.82 (s, 1H), 6.72 (d, J = 4 Hz, 1H), 6.50 (d, J = 4 Hz, 1H), 3.75–3.70 (m, 6H), 3.42 (brs, 2H). ^{13}C NMR (100 MHz, DMSO-d_6) δ:173.28, 162.57, 158.49, 153.41, 152.28, 150.23, 143.96, 114.36, 109.32, 108.24, 102.80, 100.47, 66.30, 45.45, 44.61. HRMS calcd for $C_{18}H_{16}NO_8$ $[M+H]^+$, 374.0864; found, 374.0870.

*4.1.2.5. 3,6,7-trihydroxy-9-oxo-9H-xanthen-1-yl diphenylcarbamate (**XWJ5**).* Treatment of diphenylcarbamic chloride as outlined in general procedure A provided **XWJ5** as light yellow solids in 27.5% yield. mp: > 250 °C, ESI-MS(*m/z*): 456.24 $[M+H]^+$. ^1H NMR (400 MHz, DMSO-d_6) δ: 11.00 (brs, 1H), 10.52 (brs, 1H), 9.68 (brs, 1H), 7.64 (brs, 2H), 7.42 (m, 7H), 7.28 (m, 2H), 6.84 (s, 1H), 6.73 (d, J = 4 Hz, 1H), 6.52 (d, J = 4 Hz, 1H). ^{13}C NMR (100 MHz, DMSO-d_6) δ:173.26, 162.63, 158.52, 153.48, 152.33, 151.60, 150.29, 144.04, 129.50, 114.30, 109.36, 108.08, 102.83, 100.78. HRMS calcd for $C_{26}H_{18}NO_7$ $[M+H]^+$, 456.1073; found, 456.1078.

*4.1.3. General procedure B for the synthesis of 1,6,7-trihydroxy-9-oxo-9H-xanthen-3-yl carbamate (**XWJ6**- **XWJ10**)*

A mixture of Norathyriol (6.0 g, 23.1 mmol) and 2-chlorodiphenylmethane (7.0 mL, 36.5 mmol) in the presence of diphenyl ether (5 mL) was stirred and refluxed for 2 h. Then the mixture was poured into petroleum ether (500 mL). The resulting precipitates were collected and then dried, which led to the production of the intermediate, i.e. 7,9-dihydroxy-2,2-diphenyl-10*H*-[1,3]dioxolo[4,5-*b*]xanthen-10-one.

The intermediate from the above step (424 mg, 1.0 mmol), potassium carbonate (210 mg, 1.5 mmol) and carbamic chloride (224.37 mg, 1.5 mmol) were dissolved in acetone (15 mL). The mixture was heated to 60 °C for 8 h. The solvent was evaporated and the intermediate, i.e. 9-hydroxy-10-oxo-2,2-diphenyl-10*H*-[1,3]dioxolo[4,5-*b*]xanthen-7-yl carbamate was obtained.

Pd/C (10%, 0.2 mmol) was added to a degassed solution of 9-hydroxy-10-oxo-2,2-diphenyl-10*H*-[1,3]dioxolo[4,5-*b*]xanthen-7-yl carbamate (0.2 mmol) in MeOH (15 mL) and tetrahydrofuran (5 mL), and the solution was stirred at 50 °C under H_2 (overnight). The resulting mixture was filtered and the filtrate was concentrated and purified by silica gel chromatography (hexanes and EtOAc) to provide **XWJ6**-**XWJ10**.

*4.1.3.1. 1,6,7-trihydroxy-9-oxo-9H-xanthen-3-yl dimethylcarbamate (**XWJ6**)*. Treatment of dimethylcarbamic chloride as outlined in general procedure B provided **XWJ6** as light yellow solids in 32.2% yield. m.p.: 213.0–213.9 °C. ESI-MS (*m/z*): 331.89[M + H]$^+$. ^{1}H NMR (400 MHz, DMSO-d_6) δ: 13.14 (s, 1H), 7.42 (s, 1H), 6.91 (s, 1H), 6.85 (s, 1H), 6.57 (s, 1H), 3.05 (s, 3H), 3.59 (s, 3H). ^{13}C NMR (100 MHz, DMSO-d_6) δ: 180.00, 162.12, 157.52, 156.54, 155.31, 153.27, 151.82, 144.64, 112.33, 108.31, 105.63, 104.04, 103.11, 100.93, 36.86, 36.71. HRMS calcd for $C_{16}H_{14}NO_7$ [M + H]$^+$, 332.0765; found, 332.0765.

*4.1.3.2. 1,6,7-trihydroxy-9-oxo-9H-xanthen-3-yl ethyl(methyl)carbamate (**XWJ7**)*. Treatment of ethyl(methyl)carbamic chloride as outlined in general procedure B provided **XWJ7** as light yellow solids in 33.2% yield. m.p.: 217.2–218.5 °C. ESI-MS(*m/z*): 346.30 [M + H]$^+$. ^{1}H NMR (400 MHz, DMSO-d_6) δ: 13.14 (s, 1H), 7.42 (s, 1H), 6.91 (s, 1H), 6.84 (d, *J* = 4 Hz, 1H), 6.56 (d, *J* = 4 Hz, 1H), 3.41 (q, *J* = 8 Hz, 2H), 2.97 (s, 3H), 1.12 (2 × t, *J* = 8 Hz, 3H). ^{13}C NMR (100 MHz, DMSO-d_6) δ:179.99, 162.13, 157.51, 156.55, 155.32, 152.80, 151.82, 144.60, 112.33, 108.32, 105.60, 104.05, 103.11, 100.89, 44.10, 34.48, 13.52. HRMS calcd for $C_{17}H_{16}NO_7$ [M + H]$^+$, 346.0915; found, 346.0921.

*4.1.3.3. 1,6,7-trihydroxy-9-oxo-9H-xanthen-3-yl diethylcarbamate (**XWJ8**)*. Treatment of diethylcarbamic chloride as outlined in general procedure B provided **XWJ8** as light yellow solids in 40.2% yield. m.p.: 243.3–244.3 °C. ESI-MS (*m/z*): 360.39 [M + H]$^+$, ^{1}H NMR (400 MHz, DMSO-d_6) δ: 13.14 (s, 1H), 7.43 (s, 1H), 6.92 (s, 1H), 6.85 (s, 1H), 6.57 (s, 1H), 3.40 (q, *J* = 8 Hz, 2H), 3.32 (q, *J* = 8 Hz, 2H), 1.20 (t, *J* = 8 Hz, 3H), 1.14 (t, *J* = 8 Hz,3H). ^{13}C NMR (100 MHz, DMSO-d_6) δ:180.00, 162.16, 157.54, 156.58, 155.25, 152.57, 151.82, 144.63, 112.34, 108.33, 105.60, 103.99, 103.12, 100.85, 42.39, 42.18, 14.64, 13.65. HRMS calcd for $C_{18}H_{18}NO_7$ [M + H]$^+$, 360.1071; found, 360.1078.

*4.1.3.4. 1,6,7-trihydroxy-9-oxo-9H-xanthen-3-yl morpholine-4-carboxylate (**XWJ9**)*. Treatment of morpholine-4-carbonyl chloride as outlined in general procedure B provided **XWJ9** as light yellow solids in 29.8% yield. m.p.: > 250 °C. ESI-MS (*m/z*): 374.32[M + H]$^+$. ^{1}H NMR (400 MHz, DMSO-d_6) δ: 13.18 (s, 1H), 7.42 (s, 1H), 6.89 (s, 2H), 6.61 (s, 1H), 3.68 (m, 4H), 3.59 (brs, 2H), 3.45 (brs, 2H). ^{13}C NMR (100 MHz, DMSO-d_6) δ: 179.87, 162.13, 157.26, 156.53, 155.60, 152.26, 151.90, 144.71, 112.23, 108.16, 105.73, 104.07, 103.03, 100.95, 66.17, 45.17, 44.37. HRMS calcd for $C_{18}H_{16}NO_8$ [M + H]$^+$, 374.0864; found, 374.0870.

*4.1.3.5. 1,6,7-trihydroxy-9-oxo-9H-xanthen-3-yl diphenylcarbamate (**XWJ10**)*. Treatment of diphenylcarbamic chloride as outlined in general procedure B provided **XWJ10** as light yellow solids in 32.2% yield. m.p.:126.4–126.8 °C, ESI-MS (*m/z*): 456.24[M + H]$^+$. ^{1}H NMR (400 MHz, DMSO-d_6) δ: 12.93 (s, 1H), 7.67 (s, 1H), 7.61 (m, 4H), 7.46 (m, 8H), 7.42 (m, 5H), 7.38 (s, 2H), 7.33 (s, 1H), 6.95 (s, 1H), 6.87 (d, *J* = 4 Hz, 1H), 6.61 (d, *J* = 4 Hz, 1H). ^{13}C NMR (100 MHz, DMSO-d_6) δ:180.19, 162.64, 156.83, 156.56, 154.07, 153.85, 151.74, 145.37, 141.92, 139.02, 129.68, 129.21, 128.51, 126.86, 126.26, 119.44, 118.91, 115.01, 106.18, 103.99, 102.62, 100.22, 98.04. HRMS calcd for $C_{26}H_{18}NO_7$ [M + H]$^+$, 456.1073; found, 456.1078.

*4.1.4. General procedure C for the synthesis of 6,7-dihydroxy-9-oxo-9H-xanthene-1,3-diyl biscarbamate (**XWJ11**-**XWJ14**)*

The synthetic route was similar to General Procedure B, with the only difference in mole ratio of carbamic chloride to the starting material, i.e. 7,9-dihydroxy-2,2-diphenyl-10*H*-[1,3]dioxolo[4,5-*b*]xanthen-10-one as 3.

*4.1.4.1. 6,7-dihydroxy-9-oxo-9H-xanthene-1,3-diyl bis(ethyl(methyl) carbamate) (**XWJ11**)*. Treatment of ethyl(methyl)carbamic chloride as outlined in general procedure C provided **XWJ11** as light yellow solids in 30.5% yield. m.p.: 235.6–236.5 °C, ESI-MS (*m/z*): 431.37 [M + H]$^+$, ^{1}H NMR (400 MHz, DMSO-d_6) δ: 7.36 (s, 1H), 7.31(s, 1H), 6.95 (s, 1H), 6.87 (s, 1H), 3.51–3.42 (2 × q, *J* = 8 Hz, 2H), 3.35 (q, *J* = 8 Hz, 2H), 3.11–3.06 (2 × s, 3H), 2.93 (2 × s, 3H), 1.20 (m, 6H). ^{13}C NMR (100 MHz, DMSO-d_6) δ: 173.46, 157.22, 155.13, 153.92, 153.74, 152.88, 151.67, 150.47, 144.33, 114.50, 113.40, 112.59, 109.21, 108.34, 102.80, 44.07, 34.33, 13.52, 13.15, 12.81, 12.65. HRMS calcd for $C_{21}H_{23}N_2O_8$ [M + H]$^+$, 431.1445; found, 431.1449.

*4.1.4.2. 6,7-dihydroxy-9-oxo-9H-xanthene-1,3-diyl bis(diethylcarbamate) (**XWJ12**)*. Treatment of diethylcarbamic chloride as outlined in general procedure C provided **XWJ12** as light yellow solids in 32.1% yield. m.p.: 240.8–241.7 °C. ESI-MS (*m/z*): 459.56 [M + H]$^+$. ^{1}H NMR (400 MHz, DMSO-d_6) δ: 7.36 (s, 1H), 7.31 (d, *J* = 4 Hz, 1H), 6.96 (d, *J* = 4 Hz, 1H), 6.87 (s, 1H), 3.51 (q, *J* = 8 Hz, 2H), 3.41 (q, *J* = 8 Hz, 2H), 3.34 (m, 4H), 1.30 (t, *J* = 8 Hz, 3H), 1.22 (t, *J* = 8 Hz, 3H), 1.15 (t, *J* = 8 Hz, 6H). ^{13}C NMR (100 MHz, DMSO-d_6) δ:173.37, 157.23, 155.09, 153.93, 153.36, 152.55, 151.65, 150.46, 144.32, 114.49, 113.47, 112.77, 109.19, 108.34, 102.79, 42.44, 42.14, 14.36, 13.74. HRMS calcd for $C_{23}H_{27}N_2O_8$ [M + H]$^+$, 459.1755; found, 459.1762.

*4.1.4.3. 6,7-dihydroxy-9-oxo-9H-xanthene-1,3-diyl bis(morpholine-4-carboxylate) (**XWJ13**)*. Treatment of morpholine-4-carbonyl chloride as outlined in general procedure C provided **XWJ13** as light yellow solids in 40.1% yield. m.p.: 239.8–240.2 °C. ESI –MS (*m/z*): 487.42 [M + H]$^+$. ^{1}H NMR (400 MHz, DMSO-d_6) δ: 7.39 (s, 1H), 7.37 (d, *J* = 4 Hz, 1H), 7.02 (d, *J* = 4 Hz, 1H), 6.88 (s, 1H), 3.78 (brs, 2H), 3.68 (m, 8H), 3.67 (brs, 2H), 3.46 (brs, 4H). ^{13}C NMR (100 MHz, DMSO-d_6) δ:173.50, 157.18, 155.02, 154.06, 153.03, 152.20, 151.39, 150.48, 144.42, 114.41, 113.41, 112.56, 109.15, 108.60, 102.83, 66.16, 44.60. HRMS calcd for $C_{23}H_{23}N_2O_{10}$ [M + H]$^+$, 487.1349; found, 487.1347.

*4.1.4.4. 6,7-dihydroxy-9-oxo-9H-xanthene-1,3-diyl bis(diphenylcarbamate) (**XWJ14**)*. Treatment of diphenylcarbamic chloride as outlined in general procedure C provided **XWJ14** as light yellow solids in 36.8% yield. m.p.: 247.5–248.2 °C. ESI-MS (*m/z*): 651.29 [M + H]$^+$. ^{1}H NMR (400 MHz, DMSO-d_6) δ: 7.68 (brs, 1H), 7.49–7.42 (m, 17H), 7.31 (m, 4H), 7.17 (d, *J* = 4 Hz, 1H), 6.89 (s, 1H). ^{13}C NMR (100 MHz, DMSO-d_6) δ:173.50, 157.28, 154.67, 154.22, 152.15, 151.86, 150.76, 150.59, 144.51, 142.38, 129.69, 127.46, 114.38, 113.46, 112.79, 109.30, 102.85. HRMS calcd for $C_{39}H_{27}N_2O_8$ [M + H]$^+$, 651.1758; found, 651.1762.

*4.1.5. General procedure D for the synthesis of 1,6,7-trihydroxy-3-(benzyloxy)-9H-xanthen-9-one (**XWJ15**-**XWJ26**)*

To a mixture of Norathyriol (260.0 mg, 1.0 mmol) and sodium bicarbonate (126.0 mg, 1.5 mmol) in DMF (15 mL), potassium iodide (166.0 mg, 1.0 mmol) and benzyl bromide (205.2 mg, 1.2 mmol) were added. The mixture was heated to 80 °C for 7 h. Upon completion, the mixture was cooled down to room temperature. The mixture was then diluted with ethyl acetate (20 mL), washed with H_2O (2 × 20 mL). The organic phase was dried, filtered and concentrated under reduced pressure. The residuals were purified by silica gel chromatography (hexanes and EtOAc) to provide **XWJ15**-**XWJ26**.

*4.1.5.1. 1,6,7-trihydroxy-3-((4-methylbenzyl)oxy)-9H-xanthen-9-one (**XWJ15**)*. Treatment of 4-methylbenzyl bromide as outlined in general procedure D provided **XWJ15** as white solids in 67.3% yield. m.p.: 229.5–231.6 °C. ESI-MS *m/z*: 365.24 [M + H]$^+$. ^{1}H NMR(400 MHz, DMSO-d_6) δ:13.06 (s, 1H), 10.87 (s, 1H), 9.80 (s, 1H), 7.42 (d, *J* = 4 Hz, 2H), 7.39 (s, 1H), 7.23 (t, *J* = 8 Hz, 3H), 6.35 (d, *J* = 4 Hz, 1H), 6.18 (d, *J* = 4 Hz, 1H), 5.25 (s, 2H), 2.33(s, 3H). ^{13}C NMR (100 MHz, DMSO-d_6) δ:179.35, 165.43, 163.05, 157.86, 154.40, 151.06, 144.99, 137.91, 133.51, 129.53, 128.50, 113.14, 108.20, 102.09, 101.80, 98.29, 94.06, 70.67, 21.27. HRMS calcd for $C_{21}H_{17}O_6$ [M + H]$^+$, 365.1014; found, 365.1020.

*4.1.5.2. 1,6,7-trihydroxy-3-((3-methylbenzyl)oxy)-9H-xanthen-9-one (**XWJ16**).* Treatment of 3-methylbenzyl bromide as outlined in general procedure D provided **XWJ16** as light yellow solids in 48.1% yield. m.p.: 238.0–238.6 °C. ESI-MS (*m/z*): 365.30$[M+H]^+$. ^{1}H NMR (400 MHz, DMSO-d_6) δ: 13.07 (s, 1H), 10.91 (s, 1H), 9.83 (s, 1H), 7.42 ~ 7.19 (m, 6H), 6.34 (s, 1H), 6.17 (s, 1H), 5.24 (brs, 2H), 2.34 (s, 3H). ^{13}C NMR (100 MHz, DMSO-d_6) δ:178.80, 164.71, 162.48, 162.18, 157.29, 153.86, 150.50, 144.37, 137.59, 135.88, 126.68, 128.33, 124.95, 112.60, 107.65, 101.59, 101.19, 97.69, 93.47, 70.35, 20.90. HRMS calcd for $C_{21}H_{17}O_6$ $[M+H]^+$, 365.1014; found, 365.1020.

*4.1.5.3. 1,6,7-trihydroxy-3-((2-methylbenzyl)oxy)-9H-xanthen-9-one (**XWJ17**).* Treatment of 2-methylbenzyl bromide as outlined in general procedure D provided **XWJ17** as light yellow solids in 49.2% yield. m.p.: 245.2–245.7 °C, ESI-MS (*m/z*): 363.33 $[M-H]^+$. ^{1}H NMR (400 MHz, DMSO-d_6)δ: 13.07 (s, 1H), 9.89 (brs, 2H), 7.48 (d, J = 8 Hz, 1H), 7.43 (s, 1H), 7.30 (s, 1H), 7.28 – 7.21 (m, 3H), 6.35 (d, J = 4 Hz, 1H), 6.17 (d, J = 4 Hz, 1H), 5.26 (s, 2H), 2.36 (s, 3H). ^{13}C NMR (100 MHz, DMSO-d_6)δ: 179.34, 165.52, 163.10, 157.90, 154.50, 151.13, 144.96, 137.39, 134.53, 130.66, 129.15, 128.82, 126.30, 113.21, 108.18, 102.09, 101.79, 98.31, 94.06, 69.59, 18.94. HRMS calcd for $C_{21}H_{17}O_6$ $[M+H]^+$, 365.1014; found, 365.1020.

*4.1.5.4. 3-((4-chlorobenzyl)oxy)-1,6,7-trihydroxy-9H-xanthen-9-one (**XWJ18**).* Treatment of 4-chlorobenzyl bromide as outlined in general procedure D provided **XWJ18** as white solids in 32.8% yield. m.p.: 247.5–248.2 °C. ESI-MS (*m/z*): 385.20 $[M+H]^+$. ^{1}H NMR (400 MHz, DMSO-d_6) δ:13.05(s, 1H), 10.91 (s,1H), 9.89 (s, J = 8 Hz, J = 12 Hz, 4H), 7.23 (s, 1H), 6.35 (d, J = 4 Hz, 1H), 6.18 (d, J = 4 Hz, 1H), 5.30 (s, 2H). ^{13}C NMR (100 MHz, DMSO-d_6) δ:179.38, 165.01, 163.0, 162.85, 157.82, 154.05, 151.09, 145.12, 135.63, 133.19, 130.18, 129.01, 113.33, 108.33, 101.89, 98.21, 94.10, 69.88. HRMS calcd for $C_{20}H_{14}ClO_6$ $[M+H]^+$, 385.0466; found, 385.0473.

*4.1.5.5. 3-((3-chlorobenzyl)oxy)-1,6,7-trihydroxy-9H-xanthen-9-one (**XWJ19**).* Treatment of 3-chlorobenzyl bromide as outlined in general procedure D provided **XWJ19** as white solids in 32.8% yield. m.p.: > 250 °C. ESI-MS (*m/z*): 385.14 $[M+H]^+$. ^{1}H NMR (400 MHz, DMSO-d_6) δ:13.05 (s, 1H), 10.94 (brs, 1H), 9.87 (brs, 1H), 7.61–7.44 (m, 6H), 6.35 (d, J = 4 Hz, 1H), 6.18 (d, J = 4 Hz, 1H), 5.32 (s, 1H). ^{13}C NMR (100 MHz, DMSO-d_6) δ: 179.37, 165.38, 163.05, 157.87, 154.06, 151.02, 144.88, 139.14, 133.65, 130.93, 128.52, 127.99, 126.84, 113.39, 109.98, 108.41, 101.88, 98.28, 94.12, 69.80. HRMS calcd for $C_{20}H_{14}ClO_6$ $[M+H]^+$, 385.0467; found, 385.0473.

*4.1.5.6. 3-((2-chlorobenzyl)oxy)-1,6,7-trihydroxy-9H-xanthen-9-one (**XWJ20**).* Treatment of 2-chlorobenzyl bromide as outlined in general procedure D provided **XWJ20** as yellow solids in 35.4% yield. m.p.: > 250 °C. ESI-MS (*m/z*): 383.29 $[M-H]^+$. ^{1}H NMR (400 MHz, DMSO-d_6) δ: 13.05 (s, 1H), 10.93 (brs, 1H), 9.89 (brs, 1H), 7.68 (m, 1H), 7.56 (m, 1H), 7.46–7.43 (m, 3H), 7.29(S, 1H), 6.36 (d, J = 4 Hz, 1H), 6.18 (d, J = 4 Hz, 1H), 5.33(s, 2H). ^{13}C NMR (100 MHz, DMSO-d_6) δ:179.38, 165.39, 163.06, 157.89, 154.21, 151.06, 144.91, 133.92, 133.35, 130.95, 130.70, 129.93, 127.94, 113.42, 108.34, 102.19, 101.81, 98.29, 94.07, 68.48. HRMS calcd for $C_{20}H_{14}ClO_6$ $[M+H]^+$, 385.0464; found, 385.0489.

*4.1.5.7. 3-((4-fluorobenzyl)oxy)-1,6,7-trihydroxy-9H-xanthen-9-one (**XWJ21**).* Treatment of 4-fluorobenzyl bromide as outlined in general procedure D provided **XWJ21** as light yellow solids in 34.8% yield. m.p.: > 250 °C. ESI-MS (*m/z*): 369.47 $[M+H]^+$. ^{1}H NMR (400 MHz, DMSO-d_6) δ: 13.05 (s, 1H), 7.59–7.56 (m, 2H), 7.42 (s, 1H), 7.29–7.25 (m, 3H), 6.35 (d, J = 4 Hz, 1H), 6.18 (d, J = 4 Hz, 1H), 5.28 (s, 2H). ^{13}C NMR (100 MHz, DMSO-d_6) δ:179.35, 165.46, 163.63, 163.05, 162.75, 161.21, 157.87, 154.24, 151.06, 144.93, 132.80, 130.70, 115.94, 113.26, 108.28, 102.13, 101.85, 98.30, 94.07, 70.04. HRMS calcd for $C_{20}H_{14}FO_6$ $[M+H]^+$, 369.0763; found, 369.0769.

*4.1.5.8. 3-((3-fluorobenzyl)oxy)-1,6,7-trihydroxy-9H-xanthen-9-one (**XWJ22**).* Treatment of 3-fluorobenzyl bromide as outlined in general procedure D provided **XWJ22** as light yellow solids in 44.8% yield. m.p.: > 250 °C. ESI-MS (*m/z*): 369.35 $[M+H]^+$. ^{1}H NMR (400 MHz, DMSO-d_6) δ: 13.05 (s, 1H), 7.64 (t, J = 4 Hz, 1H), 7.49–7.47 (m, 1H), 7.43 (s, 1H), 7.32–7.26 (m, 3H), 6.36 (d, J = 4 Hz, 1H), 6.18 (d, J = 4 Hz, 1H), 5.31 (s, 2H). ^{13}C NMR (100 MHz, DMSO-d_6) δ:179.38, 165.44, 163.06, 162.22, 159.77, 157.89, 154.24, 151.07, 144.88, 131.54, 125.08, 123.46, 116.06, 113.36, 108.29, 102.17, 101.76, 98.30, 94.08, 65.17. HRMS calcd for $C_{20}H_{14}FO_6$ $[M+H]^+$, 369.0763; found, 369.0769.

*4.1.5.9. 3-((2-fluorobenzyl)oxy)-1,6,7-trihydroxy-9H-xanthen-9-one (**XWJ23**).* Treatment of 2-fluorobenzyl bromide as outlined in general procedure D provided **XWJ23** as light yellow solids in 36.4% yield. m.p.: > 250 °C. ESI-MS (*m/z*): 369.19 $[M+H]^+$. ^{1}H NMR (400 MHz, DMSO-d_6) δ: 13.04 (s, 1H), 7.51–7.45 (m, 1H), 7.43 (s, 1H), 7.37 (t, J = 8 Hz, 2H), 7.23–7.18 (m, 2H), 6.34 (d, J = 4 Hz, 1H), 6.18 (d, J = 4 Hz, 1H), 5.32 (s, 2H). ^{13}C NMR (100 MHz, DMSO-d_6) δ:179.35, 171.91, 165.49, 163.89, 163.05, 161.47, 157.83, 154.08, 151.02, 144.93, 139.45, 131.08, 124.19, 115.25, 113.39, 108.41, 101.89, 98.26, 94.08, 69.87. HRMS calcd for $C_{20}H_{14}FO_6$ $[M+H]^+$, 369.0763; found, 369.0769.

*4.1.5.10. 3-((3-chloro-2-fluorobenzyl)oxy)-1,6,7-trihydroxy-9H-xanthen-9-one (**XWJ24**).* Treatment of 3-chloro-2-fluorobenzyl bromide as outlined in general procedure D provided **XWJ24** as light yellow solids in 41.6% yield. m.p.: > 250 °C. ESI-MS (*m/z*): 403.19 $[M+H]^+$. ^{1}H NMR (400 MHz, DMSO-d_6) δ: 13.04(s, 1H), 7.67–7.60(m, 2H), 7.44(s, 1H), 7.32–7.30(m, 2H), 6.35(d, J = 4 Hz, 1H), 6.18(d, J = 4 Hz, 1H), 5.36(s, 2H). ^{13}C NMR (100 MHz, DMSO-d_6) δ:179.36, 165.45, 163.06, 157.90, 157.35, 154.91, 154.03, 151.00, 144.75, 131.27, 130.06, 126.02, 125.60, 120.16, 113.53, 108.40, 101.90, 98.34, 94.15, 65.11. HRMS calcd for $C_{20}H_{13}ClFO_6$ $[M+H]^+$, 403.0374; found, 403.0379.

*4.1.5.11. 1-hydroxy-3,6,7-tris((4-methylbenzyl)oxy)-9H-xanthen-9-one (**XWJ25**).* Treatment of an excessive amount of 4-methylbenzyl bromide as outlined in general procedure D provided **XWJ25** as light yellow solids in 33.5% yield. m.p.: 180.2–180.7 °C, ESI-MS (*m/z*): 573.22 $[M+H]^+$. ^{1}H NMR (400 MHz, DMSO-d_6) δ: 13.02 (s, 1H), 7.68 (s, 1H), 7.42–7.35(m, 6H), 7.26–7.22 (m, 6H), 6.92 (s, 1H), 6.46 (d, J = 4 Hz, 1H), 6.44 (d, J = 4 Hz, 1H), 5.27 (s, 2H), 5.23 (s, 2H), 5.12 (s, 2H), 2.42 (m, 9H). ^{13}C NMR (100 MHz, DMSO-d_6) δ:179.80, 165.11, 163.22, 157.69, 155.39, 152.43, 146.22, 138.26, 138.09, 137.80, 133.46, 132.80, 132.70, 129.45, 129.29, 127.72, 127.52, 127.22, 113.51, 107.53, 103.63, 101.45, 97.67, 93.35, 71.21, 71.02, 70.41, 21.26. HRMS calcd for $C_{37}H_{33}O_6$ $[M+H]^+$, 573.2271; found, 573.2272.

*4.1.5.12. 3,6,7-tris((4-chlorobenzyl)oxy)-1-hydroxy-9H-xanthen-9-one (**XWJ26**).* Treatment of an excessive amount of 4-chlorobenzyl bromide as outlined in general procedure D provided **XWJ26** as light yellow solids in 21.6% yield. m.p.: 213.2–213.7 °C. ESI-MS (*m/z*): 633.34 $[M+H]^+$. ^{1}H NMR (400 MHz, DMSO-d_6) δ: 12.97(s, 1H), 7.68 (s, 1H), 7.46–7.39 (m, 12H), 6.92 (s, 1H), 6.46 (d, J = 4 Hz, 1H), 6.44 (d, J = 4 Hz, 1H), 5.26 (s, 2H), 5.23 (s, 2H), 5.14 (s, 2H). ^{13}C NMR (100 MHz, DMSO-d_6) δ:179.73, 164.86, 163.33, 157.62, 154.92, 152.35, 145.82, 134.85, 134.30, 133.90, 129.04, 128.84, 128.72, 128.50, 113.76, 107.55, 103.78, 101.51, 97.68, 93.44, 70.54, 70.37, 69.65. HRMS calcd for $C_{34}H_{24}Cl_3O_6$ $[M+H]^+$, 633.0628; found, 633.0633.

4.2. In vitro PTPs bioassay

4.2.1. General protocol

All the Norathyriol derivatives were tested for their inhibition of PTP1B activity by using the bioassay method developed by Sotoud, H. et al.. [27]. The compounds were firstly tested at the concentration of 10 μM. The compounds with inhibition rates greater than 50% at 10 μM were deemed as hits and were tested at nine concentrations ranging from 10 nM to 100 μM, based on which the IC_{50} values were determined. The most potent compound was further tested for its kinetics of PTP1B inhibition and its selectivity to PTP1B over other PTPs, i.e. TC-PTP, SHP2 and PTP-LAR. All the assays in this study were performed in duplicate for each concentration. Na_3VO_4 was used as a positive drug in PTPs enzymatic assays, while TCS 401 was used as the positive drug in PTP1B kinetics assay.

4.2.2. PTP1B enzymatic assay

All the test compounds including Na_3VO_4 were dissolved with 10% DMSO as stock solutions (10 mM). Prior to use, (1) compound dilutions at ten times the tested concentration(s) were prepared from the stock solutions with 10% DMSO; (2) assay buffer was prepared according to the following formula: 3-morpholinopropanesulfonic acid (MOPS, 25 mM, pH 7.0), NaCl (50 mM), Tween 20 (0.05%) and Dithiothreitol (DTT, 3 mM); (3) the substrate, i.e. 6,8-Difluoro-4-Methylumbelliferyl Phosphate (DiFMUP) dissolved in 10% DMSO (stock solution) was diluted to 100 μM with the assay buffer. To initiate the enzymatic reaction, 5 μL substrate dilutions and 5 μL compound dilutions were sequentially added to 30 μL assay buffer. Then, 10 μL PTP1B (15 ng) was added to make a 50 μL reaction mixture (DiFMUP, 10 μM; PTP1B, 15 ng; compound in 1% DMSO). After its incubation at room temperature for 30 min, fluorescence intensity (FI) of the reaction mixture was measured at an excitation wavelength of 358 nm and an emission wavelength of 455 nm using a Tecan Infinite M1000 microplate reader. The enzymatic activity (%) was calculated to measure the inhibitory effect of the compound by the following formula, i.e. activity (%) = $\{(FI_{cmpd}–FI_{blank})/(FI_{no\_cmpd}–FI_{blank})\} \times 100$ (%). Herein, FI_{cmpd} refers to FI of the mixture with the compound while FI_{blank} means FI of the mixture with no enzyme. FI_{no_cmpd} represents FI of the mixture with the enzyme and no compound. IC_{50} values were calculated based on activity values at nine concentrations, using nonlinear regression with normalized dose-response fit in GraphPad Prism 5 software (GraphPad Software Inc., La Jolla, CA).

4.2.3. PTP1B kinetics assay

Unlike PTP1B enzymatic assay that used a fixed concentration of DiFMUP (i.e. 10 μM), PTP1B kinetics assay required different concentrations of DiFMUP. In this assay, the stock solution of DiFMUP was diluted to five times the tested concentrations with the assay buffer, i.e. 25 μM, 50 μM, 100 μM, 200 μM, 400 μM, 800 μM, respectively. For each concentration, 40 μL dilutions of DiFMUP were taken and added to wells of 96-well plates. Then, 10 μL compound dilutions at the concentrations of 0 μM (10% DMSO), 2 μM, 6 μM and 18 μM were respectively added to each well that contained 40 μL DiFMUP dilutions. Lastly, 50 μL PTP1B (0.3 μg/mL) diluted in assay buffer was added to the well so as to initiate the reaction. Likewise, the reaction mixtures without the compound/the enzyme were set as two controls. The plate reader recorded the FI value of the reaction mixture in each well every two minutes and eventually calculated enzymatic velocity of the enzymatic reaction based on the time-FI plot. The Lineweaver − Burk plot was generated by GraphPad Prism 5 to determine the type of PTP1B inhibition.

4.2.4. Other PTPs enzymatic assay

The assay methods for TC-PTP, SHP2 and PTP-LAR were the same with that for PTP1B, except for the amount of the enzyme in the 50 μL reaction mixture. The amounts of TCPTP, SHP2 and PTP-LAR used for the enzymatic reactions were 0.03 ng, 0.05 ng and 0.05 ng, respectively.

4.3. Molecular docking

An X-ray structure of PTP1B for *Homo Sapiens* was downloaded from the PDB (ID: 1Q1M, 2.6 Å). All the water molecules were removed from the structure. The “Clean Protein” module of Discovery Studio was used to correct problems in the protein structure such as nonstandard names, alternative conformations and incomplete residues, standardize atom order in amino acids, modify all hydrogen atoms, correct connectivity and bond orders, modify terminal residues and generate protonation state at pH 7.0. OEDocking (version 3.0.1; OpenEye Scientific Software, Inc., Santa Fe, NM, USA) was used to convert the prepared protein to be the receptor for molecular docking, in which the binding site was defined by the cognate ligand from the structure [28–30].

The chemical structures of ligands for molecular docking were firstly drawn by ChemDraw Ultra 14.0 and then prepared using the “Prepare Ligands” module of Discovery Studio (version 2017, Dassault Systèmes BIOVIA, San Diego, USA). With this module, hydrogen atoms were added and the protonated state at the pH range of 7.3–7.5 was generated.

A maximum of 200 conformers of each prepared ligand were generated by OMEGA (version 2.5.1.4; OpenEye Scientific Software, Inc., Santa Fe, NM, USA) [31]. Then, they were docked against the PTP1B receptor by OEDocking and 10 top-scoring poses were kept. Lastly, the binding poses were visually inspected and the pose that was consistent with the SAR was picked.

5. Notes

The authors declare no competing financial interest.

Acknowledgements

This work was supported by National Natural Science Foundation of China (Grant No. 81603027) and the CAMS Innovation Fund for Medical Sciences (Grant No. 2017-I2M-1-012). We also thank “Universities and Colleges Key Programs for Foreign Talent” of State Administration of Foreign Experts Affairs P.R. China (Grant No. T2017069). We are grateful to OpenEye Scientific Software for providing an academic license for their packages and the support by District of Columbia Developmental Center for AIDS Research (Grant No. P30AI087714).

Appendix A. Supplementary material

Supplementary data to this article can be found online at https://doi.org/10.1016/j.bioorg.2019.01.059.

References

[1] A. Alonso, J. Sasin, N. Bottini, I. Friedberg, I. Friedberg, A. Osterman, A. Godzik, T. Hunter, J. Dixon, T. Mustelin, Protein tyrosine phosphatases in the human genome, Cell 117 (6) (2004) 699–711.
[2] R.J. He, Z.H. Yu, R.Y. Zhang, Z.Y. Zhang, Protein tyrosine phosphatases as potential therapeutic targets, Acta Pharmacol. Sin. 35 (10) (2014) 1227–1246.
[3] Z.Y. Zhang, Protein tyrosine phosphatases: prospects for therapeutics, Curr. Opin. Chem. Biol. 5 (4) (2001) 416–423.
[4] R. Roskoski, A historical overview of protein kinases and their targeted small molecule inhibitors, Pharmacol. Res. 100 (2015) 1–23.
[5] S.M. Stanford, N. Bottini, Targeting tyrosine phosphatases: time to end the stigma, Trends Pharmacol. Sci. 38 (6) (2017) 524–540.
[6] N.K. Tonks, C.D. Diltz, E.H. Fischer, Characterization of the major protein-tyrosine-phosphatases of human placenta, J. Biol. Chem. 263 (14) (1988) 6731–6737.
[7] Z.Y. Zhang, S.Y. Lee, PTP1B inhibitors as potential therapeutics in the treatment of type 2 diabetes and obesity, Expert Opin. Invest. Drugs 12 (2) (2003) 223–233.
[8] J.C. Byon, A.B. Kusari, J. Kusari, Protein-tyrosine phosphatase-1B acts as a negative regulator of insulin signal transduction, Mol. Cell. Biochem. 182 (1–2) (1998) 101–108.
[9] M. Elchebly, P. Payette, E. Michaliszyn, W. Cromlish, S. Collins, A.L. Loy,

D. Normandin, A. Cheng, J. Himms-Hagen, C.C. Chan, C. Ramachandran, M.J. Gresser, M.L. Tremblay, B.P. Kennedy, Increased insulin sensitivity and obesity resistance in mice lacking the protein tyrosine phosphatase-1B gene, Science 283 (5407) (1999) 1544–1548.
[10] S. Verma, S. Sharma, Protein tyrosine phosphatase as potential therapeutic target in various disorders, Curr. Molec. Pharmacol. 11 (3) (2018) 191–202.
[11] P.J. Chen, S.P. Cai, C. Huang, X.M. Meng, J. Li, Protein tyrosine phosphatase 1B (PTP1B): a key regulator and therapeutic target in liver diseases, Toxicology 337 (2015) 10–20.
[12] P.A. Thiebaut, M. Besnier, E. Gomez, V. Richard, Role of protein tyrosine phosphatase 1B in cardiovascular diseases, J. Mol. Cell. Cardiol. 101 (2016) 50–57.
[13] S.C. Yip, S. Saha, J. Chernoff, PTP1B: a double agent in metabolism and oncogenesis, Trends Biochem. Sci. 35 (8) (2010) 442–449.
[14] L. Lessard, M. Stuible, M.L. Tremblay, The two faces of PTP1B in cancer, BBA 1804 (3) (2010) 613–619.
[15] N. Krishnan, K. Krishnan, C.R. Connors, M.S. Choy, R. Page, W. Peti, L. Van Aelst, S.D. Shea, N.K. Tonks, PTP1B inhibition suggests a therapeutic strategy for Rett syndrome, J. Clin. Investig. 125 (8) (2015) 3163–3177.
[16] S. Qian, M. Zhang, Y. He, W. Wang, S. Liu, Recent advances in the development of protein tyrosine phosphatase 1B inhibitors for Type 2 diabetes, Future Med. Chem. 8 (11) (2016) 1239–1258.
[17] A.K. Tamrakar, C.K. Maurya, A.K. Rai, PTP1B inhibitors for type 2 diabetes treatment: a patent review (2011–2014), Expert Opin. Ther. Pat. 24 (10) (2014) 1101–1115.
[18] B.T. Zhao, D.H. Nguyen, D.D. Le, J.S. Choi, B.S. Min, M.H. Woo, Protein tyrosine phosphatase 1B inhibitors from natural sources, Arch. Pharmacal Res. 41 (2) (2018) 130–161.
[19] J. Li, M. Malakhova, M. Mottamal, K. Reddy, I. Kurinov, A. Carper, A. Langfald, N. Oi, M.O. Kim, F. Zhu, C.P. Sosa, K. Zhou, A.M. Bode, Z. Dong, Norathyriol suppresses skin cancers induced by solar ultraviolet radiation by targeting ERK kinases, Cancer Res. 72 (1) (2012) 260–270.
[20] J. Lei, C. Zhou, H. Hu, L. Hu, M. Zhao, Y. Yang, Y. Chuai, J. Ni, J. Cai, Mangiferin aglycone attenuates radiation-induced damage on human intestinal epithelial cells, J. Cell. Biochem. 113 (8) (2012) 2633–2642.
[21] F. Wang, J. Yan, Y. Niu, Y. Li, H. Lin, X. Liu, J. Liu, L. Li, Mangiferin and its aglycone, norathyriol, improve glucose metabolism by activation of AMP-activated protein kinase, Pharm. Biol. 52 (1) (2014) 68–73.
[22] H. Ding, Y. Zhang, C. Xu, D. Hou, J. Li, Y. Zhang, W. Peng, K. Zen, C.Y. Zhang, X. Jiang, Norathyriol reverses obesity- and high-fat-diet-induced insulin resistance in mice through inhibition of PTP1B, Diabetologia 57 (10) (2014) 2145–2154.
[23] Y. Niu, J. Liu, H.Y. Liu, L.H. Gao, G.H. Feng, X. Liu, L. Li, Hypouricaemic action of mangiferin results from metabolite norathyriol via inhibiting xanthine oxidase activity, Pharm. Biol. 54 (9) (2016) 1680–1686.
[24] J. Li, M. Liu, H. Yu, W. Wang, L. Han, Q. Chen, J. Ruan, S. Wen, Y. Zhang, T. Wang, Mangiferin improves hepatic lipid metabolism mainly through its metabolite-norathyriol by modulating SIRT-1/AMPK/SREBP-1c signaling, Front. Pharmacol. 9 (2018) 201.
[25] T. Wang, M.B. Wu, R.H. Zhang, Z.J. Chen, C. Hua, J.P. Lin, L.R. Yang, Advances in computational structure-based drug design and application in drug discovery, Curr. Top. Med. Chem. 16 (9) (2016) 901–916.
[26] R.L.M. van Montfort, P. Workman, Structure-based drug design: aiming for a perfect fit, Essays Biochem. 61 (5) (2017) 431–437.
[27] H. Sotoud, P. Gribbon, B. Ellinger, J. Reinshagen, P. Boknik, L. Kattner, A. El-Armouche, T. Eschenhagen, Development of a colorimetric and a fluorescence phosphatase-inhibitor assay suitable for drug discovery approaches, J. Biomol. Screen. 18 (8) (2013) 899–909.
[28] M.R. McGann, H.R. Almond, A. Nicholls, J.A. Grant, F.K. Brown, Gaussian docking functions, Biopolymers 68 (1) (2003) 76–90.
[29] M. McGann, FRED pose prediction and virtual screening accuracy, J. Chem. Inf. Model. 51 (3) (2011) 578–596.
[30] G.B. McGaughey, R.P. Sheridan, C.I. Bayly, J.C. Culberson, C. Kreatsoulas, S. Lindsley, V. Maiorov, J.F. Truchon, W.D. Cornell, Comparison of topological, shape, and docking methods in virtual screening, J. Chem. Inf. Model. 47 (4) (2007) 1504–1519.
[31] P.C. Hawkins, A.G. Skillman, G.L. Warren, B.A. Ellingson, M.T. Stahl, Conformer generation with OMEGA: algorithm and validation using high quality structures from the Protein Databank and Cambridge Structural Database, J. Chem. Inf. Model. 50 (4) (2010) 572–584.